Computer-Generated Tie-Dyeing using a 3D Diffusion Graph

Yuki Morimoto* and Kenji Ono

RIKEN

Abstract. Hand dyeing generates artistic representations with unique and complex patterns. The aesthetics of dyed patterns on a cloth originate from the physical properties of dyeing in the cloth and the geometric operations of the cloth. Although many artistic representations have been studied in the field of non-photorealistic rendering, dyeing remains a challenging and attractive topic. In this paper, we propose a new framework for simulating dyeing techniques that considers the geometry of the folded cloth. Our simulation framework of dyeing in folded woven cloth is based on a novel dye transfer model that considers diffusion, adsorption, and supply. The dye transfer model is discretized on a 3D graph to approximate the folded woven cloth designed by user interactions. We also develop new methods for dip dyeing and tie-dyeing effects. Comparisons of our simulated results with real dyeing demonstrate that our simulation is capable of representing characteristics of dyeing.

1 Introduction

Since ancient times, dyeing has been employed to color fabrics in both industry and arts and crafts. Various dyeing techniques are practiced throughout the world, such as wax-resist dyeing (*batik dyeing*), hand drawing with dye and paste (*Yuzen dyeing*), and many other techniques [1, 2]. Tie-dyeing produces beautiful and unique dyed patterns. The tie-dyeing process involves performing various geometric operations on a support medium, then dipping the medium into a dyebath. The process of dipping a cloth into a dyebath is called dip dyeing.

The design of dye patterns is complicated by factors such as dye transfer and cloth deformation. Professional dyers predict final dye patterns based on heuristics; they tap into years of experience and intimate knowledge of traditional dyeing techniques. Furthermore, the real dyeing process is time-consuming. For example, clamp resist dyeing requires the dyer to fashion wooden templates to press the cloth during dyeing. Templates used in this technique can be very complex. Hand dyed patterns require the dyer's experience, skill, and effort, which are combined with the chemical and physical properties of the materials. This allows the dyer to generate interesting and unique patterns. There are no other painting techniques that are associated with the deformation of the support medium. In contrast to hand dyeing, dyeing simulation allow for an inexpensive, fast, and accessible way to create dyed patterns. We focus on folded cloth geometry and dye transfer phenomenon. Figure 1 shows the simulated results obtained using our physics-based dyeing framework and a real dyed pattern.

* e-mail: yu-ki@riken.jp

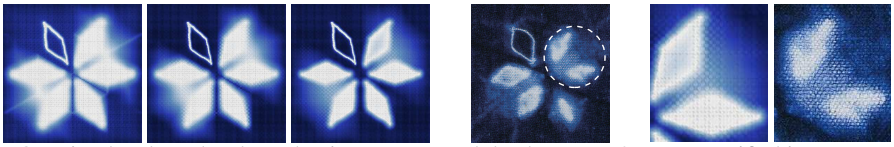

Fig. 1. Comparisons of our simulated results with a real dyed pattern.

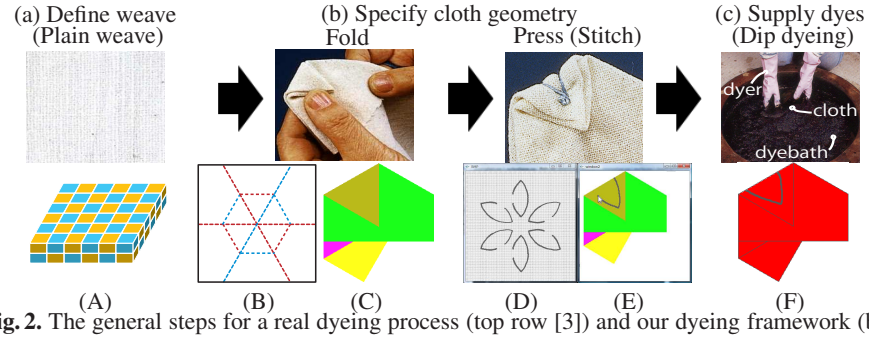

Fig. 2. The general steps for a real dyeing process (top row [3]) and our dyeing framework (bottom row) using the Chinese flower resist technique. (A) The woven cloth has a plain weave; the blue and yellow cells indicate the warp and the weft. (B) The unfolded cloth with user specified fold lines, the red and blue lines indicate ridges and valleys, and folds in the cloth. (C) The corresponding folded cloth in (B). (D, E) The interfaces representing user drawings on an unfolded and folded cloth. The gray lines indicate a user-specified boundary domain; these will be the dye resist regions. (F) The folded cloth with the red region indicating the exterior surfaces.

Related work. Non-photorealistic rendering (NPR) methods for painting and transferring pigments on paper have been developed for watercolor and Chinese ink paintings [4–9]. These methods are often based on fluid mechanics: Kunii et al. [5] used Fick's second law of diffusion to describe water spreading on dry paper with pigments; Curtis et al. [9] developed a technique for simulating watercolor effects; Chu and Tai [7] presented a real-time drawing algorithm based on the lattice Boltzmann equation ; and Xu et al. [8] proposed a generic pigment model based on rules and formulations derived from studies of adsorption and diffusion in surface chemistry and the textile industry.

Several studies have also investigated dyeing methods: Wyvill et al. [10] proposed an algorithm for rendering cracks in *batik* that is capable of producing realistic crack patterns in wax; Shamey et al. [11] used a numerical simulation of the dyebath to study mass transfer in a fluid influenced by dispersion; and Morimoto et al. [12] used a diffusion model that includes adsorption to reproduce the details of dyeing characteristics such as thin colored threads by considering the woven cloth, based on dye physics.

However, the above methods are insufficient for simulating advanced dyeing techniques, such as tie-dyeing. Previous methods are strictly 2D, and are not designed to handle the folded 3D geometry of the support medium. There is no other simulation method that considers the folded 3D geometry of the support medium which clearly affects real dyeing results. In addition, the above methods cannot be used in tandem with texture synthesis [13] to generate dyed patterns, because dyeing is a time variant physi-

cal phenomenon. Because of the large number of dyeing factors (chemical and physical phenomenon with the dyer's design, skill, and experience), only physics-based models will be capable of simulating sensitive dyeing processes. We extend the physical 2D dyeing model (Morimoto et al. [12]) to consider the folded cloth geometry.

Real dyeing process and framework overview. Figure 2 depicts the framework with a corresponding dyeing process. In the real process, the cloth is prepared, folded, and pressed to form the cloth geometry that allows resist dyeing to occur in some parts of the cloth; tie-dyeing techniques (folding, stitching, clamping, etc) are coordinated with folding and pressing. The cloth is put into a dyebath, where dye transfer occurs. The cloth is removed from the dyebath, opened, and dried to complete dye transfer. Our framework is summarized in the bottom of Figure 2. First, we define the weave structure. Then, we model the dyeing techniques with user-specified folding and pressing. Next, we calculate the distribution of the dye supply and simulate dye transfer.

Our approach. We propose a novel simulation framework that simulates dyed patterns produced by folding the cloth. This dyeing framework is based on a new dye transfer model; it is implemented using a discrete 3D diffusion graph that approximates the folded cloth. Our dye transfer model is formulated using an evolutionary system of PDEs that accounts for diffusion with adsorption and dye supply from the dyebath.

We model the effects of pressing in tie-dyeing [1] via dye capacity maps. We model dip dyeing from a dye supply map. These maps are generated from distance fields of the exterior domain and dye resist regions of the folded cloth, respectively. The graph structure is constructed as follows. The graph vertices are sampled from a 2D cloth patch. The cloth patch is then folded along the fold lines specified by the user. The graph edges connect adjacent vertices in the folded cloth. We also incorporated the two-layered cellular cloth model of Morimoto et al. [12] to represent woven cloths.

Contributions and benefits. Our main contribution is a physically based dyeing simulation framework that accounts for the folded cloth geometry associated with various dyeing techniques. The technical contributions are a novel dye transfer model and its discretization in a 3D graph to simulate tie-dyeing and dip dyeing.

Our framework allows us to produce new stylized depictions for computer graphics. We expect the framework to have applications in real dyeing processes as a computer-aided design tool. Even dyeing neophytes would be able to generate and predict dyed patterns with minimal material and labor costs. By easing the design process, we hope to advance dyeing design and help spread the dyeing tradition around the world. Our 3D diffusion graph can be applied to simulate diffusion effects in layered objects.

2 Dye Transfer Model

Our dye transfer model accounts for the diffusion, adsorption, and supply terms of the dye as described in an equation (1). The diffusion and adsorption terms describe the dye behavior based on Fick's second law [14] and dyeing physics, respectively. The supply term enables arbitrary dye distribution for dip dyeing and user drawings.

Let $f = f(\mathbf{x}, t) \in (0, 1]$ be a dye concentration function with position vector $\mathbf{x} \in \Re^3$ and time parameter $t \geq 0$, where t is independent of $\mathbf{x}$. The dyeing model is formulated by the following evolutionary system of PDEs.

$$\frac{\partial f(\mathbf{x}, t)}{\partial t} = \text{div}(D(\mathbf{x})\nabla f) + s(\mathbf{x}, f) - a(\mathbf{x}, f), \tag{1}$$

where $D(\mathbf{x})$ is the diffusion coefficient function, div$(\cdot)$ and $\nabla(\cdot)$ are the divergence and gradient operators respectively, and $s(\cdot, \cdot)$ and $a(\cdot, \cdot)$ are the source and sink terms that represent dye supply and adsorption, whereas div$(D(\mathbf{x})\nabla f)$ is the diffusion term. We model the functions $s(\cdot, \cdot)$ and $a(\cdot, \cdot)$ as follows.

$$s(\mathbf{x}, f) = \begin{cases} \alpha M_s(\mathbf{x}) \text{ if } M_s(\mathbf{x}) > f(\mathbf{x}, t) \text{ and } M_{cd}(\mathbf{x}) > f(\mathbf{x}, t). \\ 0 \qquad\qquad\qquad\qquad \text{Otherwise,} \end{cases}$$

$$a(\mathbf{x}, f) = \begin{cases} \beta f(\mathbf{x}, t) \text{ if } h(\mathbf{x}, t) < a_d(\mathbf{x}, f) \text{ and } M_{ca}(\mathbf{x}) > h(\mathbf{x}, t). \\ 0 \qquad\qquad\qquad\qquad \text{Otherwise,} \end{cases}$$

where α is the user-specified dye concentration, $M_s(\mathbf{x}) \in [0, 1]$ is the dye supply map, $M_{cd}(\mathbf{x})$ and $M_{ca}(\mathbf{x})$ are the diffusion and adsorption capacity maps, $\beta \in [0, 1]$ is the user-specified adsorption rate, and $a_d(\mathbf{x}, f)$ is the adsorption capacity according to adsorption isotherms. The adsorption isotherm depicts the amount of adsorbate on the adsorbent as a function of its concentration at constant temperature. In this paper, we employ the Langmuir adsorption model [15], which is a saturation curve, to calculate $a_d(\mathbf{x}, f)$ in our simulation based on the model developed by Morimoto et al. [12]. The adsorbed dye concentration $h(\mathbf{x}, t) \in [0, 1]$ is given by the equation bellow and the evolution of $f(\mathbf{x}, t)$ and $h(\mathbf{x}, t)$ as $t \to \infty$ describes the dyeing process.

$$\frac{\partial h(\mathbf{x}, t)}{\partial t} = a(\mathbf{x}, f)\frac{M_{cd}(\mathbf{x})}{M_{ca}(\mathbf{x})}, \tag{2}$$

Two-layered cloth model and diffusion coefficient [12]. Since the cloth is woven in wefts and warps, the layers of the cloth model naturally reflect this, and consist of a layer of weft cells and a layer of warp cells. The positions of cells are defined along the cloth weave. The diffusion coefficient $D(\mathbf{x})$ is defined between graph vertices, and is calculated from the composition of the dyestuff and cloth fibre, the style of the weave, and the relationship of cloth fibers between cells, causing an anisotropic diffusion. When considering the x-y plane, diffusion occurs between adjacent cells in the same plane. In the z-direction, diffusion is dictated by cloth geometry, which is described in more detail in Section 3.

Boundary condition. Let $\mathbf{z} \in \mathcal{B}$ be the boundary domain for dye transfer. We use the Neumann boundary condition $\frac{\partial f(\mathbf{z}, t)}{\partial \mathbf{n}(\mathbf{z})} = b(\mathbf{z}), \mathbf{z} \in \mathcal{B}$ where $\mathbf{n}(\mathbf{z})$ is a unit normal vector of the boundary. In tie-dyeing, parts of the cloth are pressed together by folding and pressing. We assume that the pressed region is the boundary domain because no space exists between the pressed cloth parts for the dye to enter. In our framework, the user specifies $\mathcal{B}$ by drawing on both the unfolded and folded cloth, as shown in Figure 2 (D) and (E), respectively. In the case of the folded cloth, shown in Figure 2 (E), we project $\mathcal{B}$ to all overlapping faces of the folded cloth. Here, the faces are the polygons of the folded cloth, as shown in Figure 2 (C).

Press function. We introduce a press function $P(\mathbf{x}, c) \in [0, 1]$ as a press effect from dyeing technique. Here c is a user-specified cut-off constant describing the domain of influence of the dye supply and the capacity maps, and represents the physical parameters. The extent of the pressing effect and dye permeation depend on the both softness and elasticity of the cloth and on the tying strength. The press function serves to;

- Limit dye supply (Pressed regions prevent dye diffusion).
- Decrease the dye capacity (Pressed regions have low porosity).

We approximate the magnitude of pressure using the distance field $dist(\mathbf{x}, \mathcal{B})$ obtained from the pressed boundary domain $\mathcal{B}$. Note that the press effect only influences the interior surfaces of the cloth, as only interior surfaces can press each other.

We define Ω as the set of exterior surfaces of the tied cloth that are in contact with the dye and $\mathcal{L}$ as the fold lines that the user input to specify the folds. We define Ω, $\mathcal{B}$, and $\mathcal{L}$ as fold features (Figure 3). We calculate the press function $P(\mathbf{x}, c)$ as described in Pseudocode 1. In Pseudocodes 1 and 2, $CalcDF()$ calculates the distance field obtained from the fold feature indicated by the first argument, and returns infinity on the fold features indicated by the second and third arguments. We use m as the number of vertices in the diffusion graph described in Section 3.

Dye supply map. The dye supply map $M_s(\mathbf{x})$ (Figure 4) describes the distribution of dye sources and sinks on the cloth, and is applied to the dye supply term in equation (1). In dip dyeing, the dye is supplied to both the exterior and interior surfaces of the folded cloth. The folded cloth opens naturally except in pressed regions, allowing liquid to enter the spaces between the folds (Figure 5). Thus, we assume that $M_s(\mathbf{x})$ is inversely proportional to the distance from Ω, as it is easier to expose regions that are closer to the liquid dye. Also, the dye supply range depends on the movement of the cloth in the dyebath. We model this effect by limiting $dist(\mathbf{x}, \Omega)$ to a cut-off constant c_Ω. Another cut-off constant $c_{\mathcal{B}_1}$ limits the influence of the press function $P(\mathbf{x}, c_{\mathcal{B}_1})$.

The method used to model the dye supply map $M_s(\mathbf{x})$ is similar to the method used to model the press function, and is described in Pseudocode 2. In Pseudocode 2, $dist_{max}$ is the max value of $dist(\mathbf{x}, \Omega)$ and $GaussFilter()$ is a Gaussian function used to mimic rounded-edge folding (as opposed to sharp-edge folding) of the cloth.

$dist(\mathbf{x}, \mathcal{B}) \leftarrow CalcDF(\mathcal{B}, \Omega, \mathcal{L})$
for i=1 to m **do**
  if $dist(i, \mathcal{B}) > c$ **then**
    $P(i, c) \leftarrow 1.0$
  else
    $P(i, c) \leftarrow dist(i, \mathcal{B})/c$
  end if
end for

Pseudocode 1. Press function.

$dist(\mathbf{x}, \Omega) \leftarrow CalcDF(\Omega, \mathcal{B}, \mathcal{L})$
for i=1 to m **do**
  $dist(i, \Omega) \leftarrow (dist_{max} - dist(i, \Omega))$
  if $dist(i, \Omega) > c_\Omega$ **then**
    $dist(i, \Omega) \leftarrow P(i, c_{\mathcal{B}_1})$
  else
    $dist(i, \Omega) \leftarrow P(i, c_{\mathcal{B}_1}) dist(i, \Omega)/c_\Omega$
  end if
end for
$M_s(\mathbf{x}) \leftarrow GaussFilter(dist(\mathbf{x}, \Omega))$

Pseudocode 2. Dye supply map.

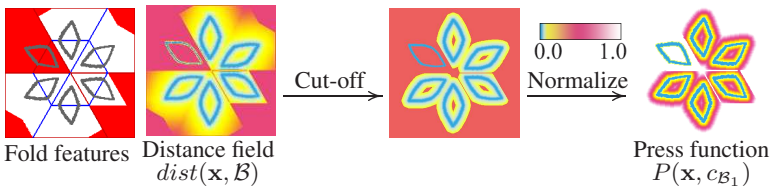

Fig. 3. An example for calculating the press function $P(\mathbf{x}, c_{\mathcal{B}_1})$ for the Chinese flower resist. In the fold features, the exterior surface Ω, pressed boundary domain $\mathcal{B}$, and the fold lines $\mathcal{L}$ are shown by red, gray, and blue colors.

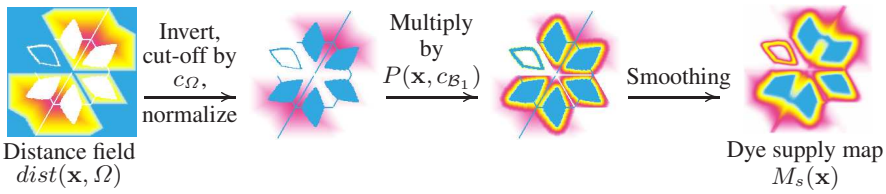

Fig. 4. An illustration of the dye supply map $M_s(\mathbf{x})$ for the Chinese flower resist.

Fig. 5. Photographs of real dip dyeing. The left shows a folded cloth pressed between two wooden plates. The right shows folded cloths that have opened naturally in liquid.

Fig. 6. Illustration for our diffusion capacity map $M_{cd}(\mathbf{x})$ calculated by taking the product of the basic capacity and $P(\mathbf{x}, c_{\mathcal{B}_2})$.

Capacity maps. The capacity maps indicate the dye capacities in a cloth; they define the spaces that dyes can occupy. We first calculate the basic capacities from a fibre porosity parameter [12]. The cut-off constant $c_{\mathcal{B}_2}$ limits the press function $P(\mathbf{x}, c_{\mathcal{B}_2})$ used here. We then multiply these capacities by the press function to obtain the capacity maps $M_{cd}(\mathbf{x})$ and $M_{ca}(\mathbf{x})$ (see Figure 6).

3 Graph Diffusion

We approximate the user-specified cloth geometry by a 3D diffusion graph $\mathcal{G}$. Our transfer model is then discretized on the graph.

Diffusion graph construction. We construct multiple two-layered cells from the two-layered cellular cloth model by cloth-folding operations. The diffusion graph $\mathcal{G}$ is a

weighted 3D graph with vertices $\mathbf{v}_i$, edges, and weights w_{ij} where $i, j = 1, 2, .., m$. The vertex $\mathbf{v}_i$ in the diffusion graph $\mathcal{G}$ is given by the cell center.

We apply the ORIPA algorithm [16], which generates the folded paper geometry from the development diagram, to the user-specified fold lines on a rectangular cloth. The fold lines divide the cloth into a set of faces as shown in Figure 2 (B). The ORIPA algorithm generates the corresponding vertex positions of faces on the folded and unfolded cloths and the overlapping relation between every two faces as shown in Figure 2 (C). We apply ID rendering to the faces to obtain the overlapping relation for multiple two-layered cells. We then determine the contact areas between cells in the folded cloth, and construct the diffusion graph $\mathcal{G}$ by connecting all vertices $\mathbf{v}_i$ to vertices $\mathbf{v}_j$ in the adjacent contact cell by edges, as illustrated in Figure 7.

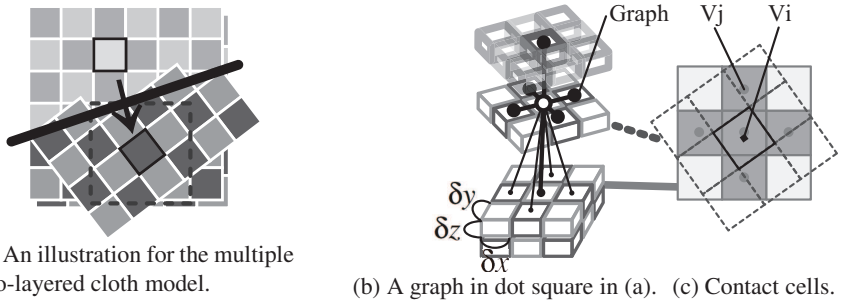

(a) An illustration for the multiple two-layered cloth model.

(b) A graph in dot square in (a). (c) Contact cells.

Fig. 7. Graph construction from folded geometry of woven cloth. The bold line in (a) represents a fold line. The gray points in (c) are contact cell vertices $\mathbf{v}_j$ of the target cell vertex $\mathbf{v}_i$.

Discretization in diffusion graph. The finite difference approximation of the diffusion term of equation (1) at vertex $\mathbf{v}_i$ of $\mathcal{G}$ is given by

$$\mathrm{div} D(\mathbf{x}) \nabla f \approx \sum_{j \in N(i)} w_{ij} \frac{f(\mathbf{v}_j, t) - f(\mathbf{v}_i, t)}{|\mathbf{v}_j - \mathbf{v}_i|^2},$$

where $w_{ij} = D_{ij} A_{ij}$, $N(i)$ is an index set of vertices adjacent to $\mathbf{v}_i$ in $\mathcal{G}$, and D_{ij} and A_{ij} are the diffusion coefficient and the contact area ratio between vertices $\mathbf{v}_i$ and $\mathbf{v}_j$, respectively (Figure 7). We calculate the distance between $\mathbf{v}_i$ and $\mathbf{v}_j$ from cell sizes, $\delta x, \delta y, \delta z$, and define $D_{ij} = (D(\mathbf{v}_i) + D(\mathbf{v}_j))/2$ between vertices connected by folding (Figure 8).

The following semi-implicit scheme gives our discrete formulation of equation (1):

$$(I - (\delta t)L)\mathbf{f}^{n+1} = \mathbf{f}^n + \delta t(\mathbf{s}^n - \mathbf{a}^n),$$

which is solved using the SOR solver [17], where I is the identity matrix, δt is the discrete time-step parameter, n is the time step, and

$$\mathbf{f}^n = \{f(\mathbf{v}_1, n), f(\mathbf{v}_2, n), .., f(\mathbf{v}_m, n)\},$$

Fig. 8. From the left to right, five D_{ij} for x, y directions in the weft layer, z direction in both the layers, and x, y directions in the warp layer and two $D(\mathbf{v}_i)$ in the weft and warp layer in our results, where $D_{max} = 2.68e-006$.

$$\mathbf{s}^n = \{s(\mathbf{v}_1, f(\mathbf{v}_1, n)), s(\mathbf{v}_2, f(\mathbf{v}_2, n)), .., s(\mathbf{v}_m, f(\mathbf{v}_m, n))\},$$
$$\mathbf{a}^n = \{a(\mathbf{v}_1, f(\mathbf{v}_1, n)), a(\mathbf{v}_2, f(\mathbf{v}_2, n)), .., a(\mathbf{v}_m, f(\mathbf{v}_m, n))\},$$

L is the mxm graph Laplacian matrix [18] of $\mathcal{G}$. The element l_{ij} of L is given by

$$l_{ij} = \begin{cases} w_{ij}/|\mathbf{v}_j - \mathbf{v}_i|^2 & \text{if } i \neq j, \\ -\sum_{j \in N(i)} l_{ij} & \text{Otherwise.} \end{cases}$$

We then simply apply the forward Euler scheme to equation (2):

$$h(\mathbf{v}_i, n+1) = h(\mathbf{v}_i, n) + \delta t a(\mathbf{v}_i, f(\mathbf{v}_i, n)) \frac{M_{cd}(\mathbf{v}_i)}{M_{ca}(\mathbf{v}_i)}$$

The diffused and adsorbed dye amounts at $\mathbf{v}_i$ are given by $f(\mathbf{v}_i, n) M_{cd}(\mathbf{v}_i)$ and $h(\mathbf{v}_i, n) M_{ca}(\mathbf{v}_i)$, respectively. The dye transfer calculation stops when the evolution of equation (1)converges to $\sum_{i=1}^{m} |f(\mathbf{v}_i, n)^n - f(\mathbf{v}_i, n)^{n-1}|/m \leq \epsilon$.

4 Results

Table 1 summarizes the parameters used in this study performed. For visualizations of the dyed cloth, we render the images by taking the product of the sum of dye (transferred and adsorbed) and its corresponding weft and warp texture.

The simulated results obtained using both large and small cut-off constants are juxtaposed in Figure 9. From (a), we can observe that with large values of c_{Ω}, the dye is able to permeate into the interior of the folded cloth, while small values of c_{Ω}, only exterior surfaces receive dye due to the softness and elasticity of the cloth. From (b), large values of cut-off constant $c_{\mathcal{B}_1}$ limit dye supply throughout the cloth while small values of $c_{\mathcal{B}_1}$ only prevent dye supply to the pressed regions of the cloth, due to cloth properties mentioned above. Essentially, reducing the cut-off constant $c_{\mathcal{B}_1}$ affects the dye supply by reducing the space between the faces of the folded cloth. From (c), large values of cut-off constant $c_{\mathcal{B}_2}$ limit dye perfusion throughout the cloth while small values of $c_{\mathcal{B}_2}$ limit it in pressed regions only. Reducing cut-off constant $c_{\mathcal{B}_2}$ modifies the capacity maps by reducing the space between fibers. These results suggest that the cut-off constants can be manipulated to generate a wide variety of possible dyeing process. In future projects, we will aim to automate the selection of these cut-off constants.

Common parameters	(Intel Core i7 (3.2 GHz) PC with 3 GB RAM and a C++ compiler)		
Boundary condition value	$b(\mathbf{z})$ =0	Initial dye condition	$f(\mathbf{x},0) = h(\mathbf{x},t)$ =0
Discrete time step	δt =0.5	Vertex number of $\mathcal{G}$	m =2x400x400
Stopping criterion	ϵ =0.00001	Cell size	$\delta x = \delta y = 0.0005$,
Dye supply constant, adsorption rate	$\alpha, \beta = 0.7, 0.1$		$\delta z = 0.005$

Other parameters and timing	Figure 9	Seikaiha	Kumo shibori	Itajime
Cut-off constant $c_\Omega, c_{\mathcal{B}_1}, c_{\mathcal{B}_2}$	100.0, 16.0, 8.0	10.0, 16.0, 8.0	140.0, 16.0, 8.0	160.0, 16.0, 8.0
Computing time (sec/time step)	/	0.445	0.476	0.372

Table 1. Parameters and timing for our results (Figure 9, 10).

Figure 10 shows real dyed cloth and our simulated results for a selection of tie-dyeing techniques. The dyeing results are evaluated by examining the color gradation, which stems from cloth geometry. Our framework is capable of generating heterogeneous dyeing results by visualizing the dye transferring process. While we cannot perform a direct comparison of our simulated results to real results, as we are unable to precisely match the initial conditions or account for other detailed factors in the dyeing process, our simulated results (a, b) corrspond well with real dyeing results (c). Since our dyeing framework enables dyeing simulations that account for the geometry of the folded cloth and advanced dyeing techniques, we can observe the characteristics of tie-dyeing as an interesting gradation in our simulated results.

Discussion. Our tie-dyeing operation does not support unintentional deformations afterwards, such as wrinkles and stretching. The *Kumo shibori* in Figure 10 shows the importance of these effects. Our folding operation results in a triangular folded cloth (e) while real tied cloth looks like a stick (d), resulting in different dyed patterns. Our result show symmetry, but real results exhibit a warped geometry. In Figure 1, the real result has petals of varying sizes, with the smallest one appearing more blurred. On the other hand, our simulated result displays uniform petal size and blurring, save for the petal on the exterior. This is likely due to thickness of the cloth.

We should develop an interactive interface to edit the dye supply and capacity maps for an intuitive designing. Air pockets that are present between cloth layers in real folded cloths could be modeled in our system by varying the graph weights.

5 Conclusion

In this paper, we describe a novel dyeing framework based on a new dye transfer model and its discrete implementation in a 3D diffusion graph that approximates a folded cloth. The framework is able to generate a wide range of dyed patterns produced using a folded cloth, which are difficult to produce by conventional methods. Since our framework is based on dyeing physics and real dyeing processes, we expect that it is not only a new graphical tool for NPR, but it can also be used as a dyeing simulator for designing.

One limitation of our framework is designing multiple dye patterns using geometric operations on a single cloths; these operations can be quite complex and unintuitive with the current method. Thus our future work will include sketch-based design interface for

dyeing. Cloth modeling using curved folds should be implemented for more complex dye patterns.

Acknowledgements

We would like to thank Prof. Hiromasa Suzuki, Prof. Yutaka Ohtake, Dr. Shin Yoshizawa, Dr. Gaku Hashimoto, and Mr. Adam Pan for their helpful comments. We also thank Asako Sakakibara and Jun Mitani. The images of real dyeing in this paper and ORIPA program are courtesy of Asako Sakakibara and Jun Mitani, respectively. This work was funded in part by a grant from the Japanese Information-Technology Promotion Agency (IPA).

References

1. Wada, Y.I.: Memory on Cloth (Shibori Now). Kodansha International Ltd. (2002)
2. Polakoff, C.: The art of tie and dye in africa. African Arts, African Studies Centre **4** (1971)
3. Sakakibara, A.: Nihon Dento Shibori no Waza (Japanese Tie-dyeing Techniques). Shiko Sha (in Japanese) (1999)
4. Bruce Gooch, A.G.: Non-Photorealistic Rendering. A K Peters Ltd (2001)
5. Kunii, T.L., Nosovskij, G.V., Vecherinin, V.L.: Two-dimensional diffusion model for diffuse ink painting. Int. J. of Shape Modeling **7** (2001) 45–58
6. Wilson, B., Ma, K.L.: Rendering complexity in computer-generated pen-and-ink illustrations. In: Proc. of Int. Symp. on NPAR, ACM (2004) 129–137
7. Chu, N.S.H., Tai, C.L.: Moxi: real-time ink dispersion in absorbent paper. ACM Trans. Graph. **24** (2005) 504–511
8. Xu, S., Tan, H., Jiao, X., Lau, W.F.C.M., Pan, Y.: A generic pigment model for digital painting. Comput. Graph. Forum **26** (2007) 609–618
9. Curtis, C.J., Anderson, S.E., Seims, J.E., Fleischer, K.W., Salesin, D.H.: Computer-generated watercolor. Computer Graphics **31** (1997) 421–430
10. Wyvill, B., van Overveld, C.W.A.M., Carpendale, M.S.T.: Rendering cracks in batik. In: NPAR. (2004) 61–149
11. Shamey, R., Zhao, X., Wardman, R.H.: Numerical simulation of dyebath and the influence of dispersion factor on dye transport. In: Proc. of the 37th conf. on Winter simulation, Winter Simulation Conference (2005) 2395–2399
12. Morimoto, Y., Tanaka, M., Tsuruno, R., Tomimatsu, K.: Visualization of dyeing based on diffusion and adsorption theories. In: Proc. of Pacific Graphics, IEEE Computer Society (2007) 57–64
13. Kwatra, V., Wei, L.Y.: Course 15: Example-based texture synthesis. In: ACM SIGGRAPH 2007 courses. (2007)
14. Fick, A.: On liquid diffusion. Jour. Sci. **10** (1855) 31–39
15. Langmuir, I.: The constitution and fundamental properties of solids and liquids. part i. solids. Journal of the American Chemical Society **38** (1916) 2221–2295
16. Mitani, J.: The folded shape restoration and the CG display of origami from the crease pattern. In: 13th international Conference on Geometry and Graphics. (2008)
17. Press, W.H., Teukolsky, S.A., Vetterling, W.T., Flannery, B.P.: Numerical recipes in C (2nd ed.): the art of scientific computing. Cambridge University Press (1992)
18. Chung, F.R.K.: Spectral Graph Theory. American Mathematical Society (1997) CBMS, Regional Conference Series in Mathematics, Number 92.

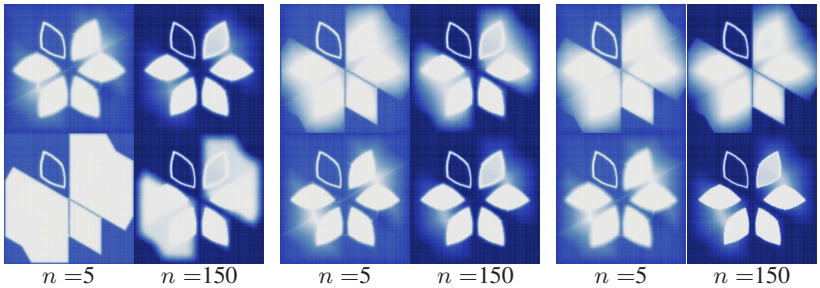

(a) c_Ω=300, 1 (top, bottom) (b) $c_{\mathcal{B}_1}$=100, 1 (top, bottom) (c) $c_{\mathcal{B}_2}$=100, 1 (top, bottom)

Fig. 9. Comparison of simulated results obtained using different cut-off constants while keeping the other parameters constant.

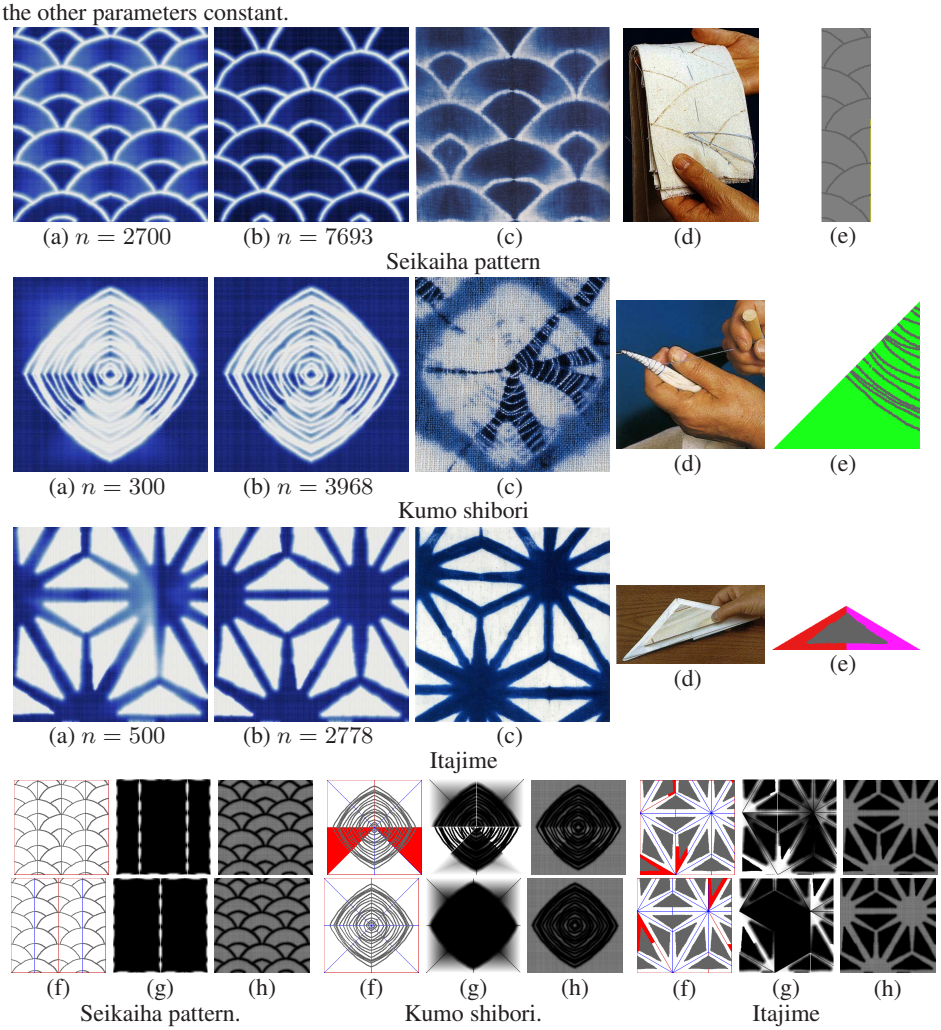

Fig. 10. Various tie-dyeing results and their corresponding conditions. (a) Our simulated results. (b) Our converged simulated results. (c) Real tie-dyeing results [3]. (d) Tie-dyeing techniques. (e) Folded cloths with user-specified boundary domains. (f) Fold features. (g) Dye supply maps $M_s(\mathbf{x})$. (h) Dye capacity maps $M_{cd}(\mathbf{x})$. In (f), (g), and (h), the top and bottom images indicate the top and bottom layers of the cloth model, respectively. The thin gray regions in the Seikaiha pattern (e) indicate regions that were covered with a plastic sheet to prevent dye supply on them; they are not the boundary domain. n is the number of time steps.